

COMPARISON BETWEEN THE ONE PIEZOELECTRIC ACTUATOR AND THE TWO ONES ON VIBRATION CONTROL OF A FLEXIBLE TWO-LINK MANIPULATOR USING FINITE ELEMENT METHOD

ABDUL KADIR MUHAMMAD¹, SHINGO OKAMOTO² & JAE HOON LEE³

¹Center for Mechatronics and Control Systems, Mechanical Engineering Department,

State Polytechnic of Ujung Pandang, Jalan Perintis Kemerdekaan KM 10, Makassar, Indonesia

^{2,3,4}Graduate School of Science and Engineering, Ehime University, 3-Bunkyo-cho, Matsuyama, Japan

ABSTRACT

The purposes of this research are to derive the equations of motion of a flexible two-link system by a finite element method, to develop computational codes in order to perform dynamics simulations with vibration control and to propose an effective control scheme of a flexible two-link manipulator. The flexible two-link manipulator used in this paper consists of two aluminum beams as flexible links, two clamp-parts, two servo motors to rotate the links and two piezoelectric actuators to control vibration. Computational codes on time history responses, FFT (Fast Fourier Transform) processing and eigenvalues - eigenvectors analysis were developed to calculate the dynamic behavior of the links. Furthermore, a control scheme using the piezoelectric actuators was designed to suppress the vibration. Two proportional-derivative controllers were designed and demonstrated their performances. The calculated results of the controlled two-link manipulator revealed that the vibration of the flexible manipulator can be controlled effectively even though only use one piezoelectric actuator.

KEYWORDS: Finite Element Method, Flexible Manipulator, Piezoelectric Actuator, Vibration Control

INTRODUCTION

Employment of flexible manipulators is recommended in the space and industrial applications in order to accomplish high performance requirements such as high-speed besides safe operation, increasing of positioning accuracy, and lower energy consumption, namely less weight. However it is not usually easy to control a flexible manipulator because of its inheriting flexibility. Deformation of the flexible manipulator when it is operated must be considered by any control. Its controller system should be dealt with not only its motion but also vibration due to the flexibility of the link.

In the past few decades, a number of modeling methods and control strategies using piezoelectric actuators to deal with the vibration problem have been investigated by researchers [1 – 7]. Nishidome and Kajiura [1] investigated a way to enhance performances of motion and vibration of a flexible-link mechanism. They used a modeling method based on modal analysis using the finite-element method. The model was described as a state space form. Their control system was constructed with a designed dynamic compensator based on the mixed of H_2/H_∞ . They recommended separating the motion and vibration controls of the system. Yavus Yaman et al [2] and Kircali et al [3] studied an active vibration control technique on aluminum beam modeled in cantilevered configuration. The studies used the ANSYS package program for modeling. They investigated the effect of element selection in finite-element modeling. The model was reduced to state

space form suitable for application of H_∞ [2] and spatial H_∞ [3] controllers to suppress vibration of the beam. They showed the effectiveness of their techniques through simulation. Zhang et al [4] has studied a flexible piezoelectric cantilever beam. The model of the beam using finite-elements was built by ANSYS application. Based on the Linear Quadratic Gauss (LQG) control method, they introduced a procedure to suppress the vibration of the beam with the piezoelectric sensors and actuators were symmetrically collocated on both sides of the beam. Their simulation results showed the effectiveness of the method. Gurses et al [5] investigated vibration control of a flexible single-link manipulator using three piezoelectric actuators. The dynamic modeling of the link had been presented using Euler-Bernoulli beam theory. Composite linear and angular velocity feedback controls were introduced to suppress the vibration. Their simulation and experimental results showed the effectiveness of the controllers. Xu and Koko [6] studied finite-element analysis and designed controller for flexible structures using piezoelectric material as actuators and sensors. They used a commercial finite-element code for modeling and completed with an optimal active vibration control in state space form. The effectiveness of the control method was confirmed through simulations. Kusculuoglu et al [7] had used a piezoelectric actuator for excitation and control vibrations of a beam. The beam and actuator were modeled using Timoshenko beam theory. An optimized vibration absorber using an electrical resistive-inductive shunt circuit on the actuator was used as a passive controller. The effectiveness of results was shown by simulations and experiment.

In the recent two years, Muhammad et al [8 – 12] have actively studied vibration control on a flexible single-link manipulator with a piezoelectric actuator using finite-element method. Model of the single-link and the piezoelectric actuator was built using one-dimensional and two-node elements. They introduced a simple and effective control scheme with the actuator using proportional (P), PD and AF controls strategies. The effectivenesses of the proposed control scheme and strategies were shown through simulations and experiments.

The purposes of this research are to derive the equations of motion of a flexible two-link system by a finite element method, to develop computational codes in order to perform dynamics simulations with vibration control and to propose an effective control scheme of a flexible two-link manipulator. The flexible two-link manipulator used in this paper consists of two aluminum beams as flexible links, two aluminum clamp-parts, two servo motors to rotate the links and two piezoelectric actuators to control vibration. Computational codes on time history responses, FFT (Fast Fourier Transform) processing and eigenvalues - eigenvectors analysis were developed to calculate the dynamic behavior of the links. An end-effector that treated as a concentrated mass was introduced to demonstrate a complete flexible two-link manipulator system. Finally, two proportional-derivative controllers were designed to suppress the vibration. They were done by adding bending moments generated by the piezoelectric actuators to the two-link system.

FORMULATION BY FINITE ELEMENT METHOD

The links have been discretized by finite elements. Every finite element (Element i -th) has two nodes namely Node i and Node $(i+1)$. Every node (Node i) has two degrees of freedom [8 - 12], namely the lateral deformation $v_i(x,t)$, and the rotational angle $\psi_i(x,t)$. The length, the cross-sectional area and the area moment of inertia around z -axis of every element are denoted by l_i , S_i and I_{zi} respectively. Mechanical properties of every element are denoted as Young's modulus E_i and mass density ρ_i .

Kinematics

Figure 1 shows the position vector r_{p1} and r_{p2} of arbitrary points P_1 and P_2 on Link 1 and Link 2 in the global and

rotating coordinate frames. Let the links as flexible beams have a motion that is confined in the horizontal plane as shown in Figure 1. The $O - XY$ frame is the global coordinate frame with Z -axis is fixed. Furthermore, $o_1 - x_1y_1$ and $o_2 - x_2y_2$ are the rotating coordinate frames fixed to the root of Link 1 and Link 2, respectively (z_1 -axis and z_2 -axis are fixed). The unit vectors in X, Y, x_1, y_1, x_2 and y_2 axes are denoted by $\mathbf{I}, \mathbf{J}, \mathbf{i}_1, \mathbf{j}_1, \mathbf{i}_2$ and \mathbf{j}_2 , respectively. The first motor is installed on the root of the Link 1. The second motor that treated as a concentrated mass is installed in the root of the Link 2. The rotational angles of the first and second motor when the links rotate are denoted by $\theta_1(t)$ and $\theta_2(t)$. Length of Link 1 is denoted by L_1 . Lateral deformation of the arbitrary points P_1 and P_2 in the first and the second links are denoted by v_{p1} and v_{p2} , respectively. Lateral deformation and rotational angel of the end-point of the first link are denoted by v_e and ψ_e , respectively. The position vector \mathbf{r}_{p1} and \mathbf{r}_{p2} of the arbitrary points P_1 and P_2 at time $t = t$, measured in the $O - XY$ frame shown in Figure 1 are expressed by

$$\mathbf{r}_{p1} = X_{p1}(x_1, \theta_1, v_{p1}, t)\mathbf{I} + Y_{p1}(x_1, \theta_1, v_{p1}, t)\mathbf{J} \quad (1)$$

$$\mathbf{r}_{p2} = X_{p2}(x_2, \theta_1, \theta_2, v_e, \psi_e, v_{p2}, t)\mathbf{I} + Y_{p2}(x_2, \theta_1, \theta_2, v_e, \psi_e, v_{p2}, t)\mathbf{J}, \quad (2)$$

where

$$X_{p1} = x_1 \cos \theta_1(t) - v_{p1}(x_1, t) \sin \theta_1(t) \quad (3)$$

$$Y_{p1} = x_1 \sin \theta_1(t) + v_{p1}(x_1, t) \cos \theta_1(t) \quad (4)$$

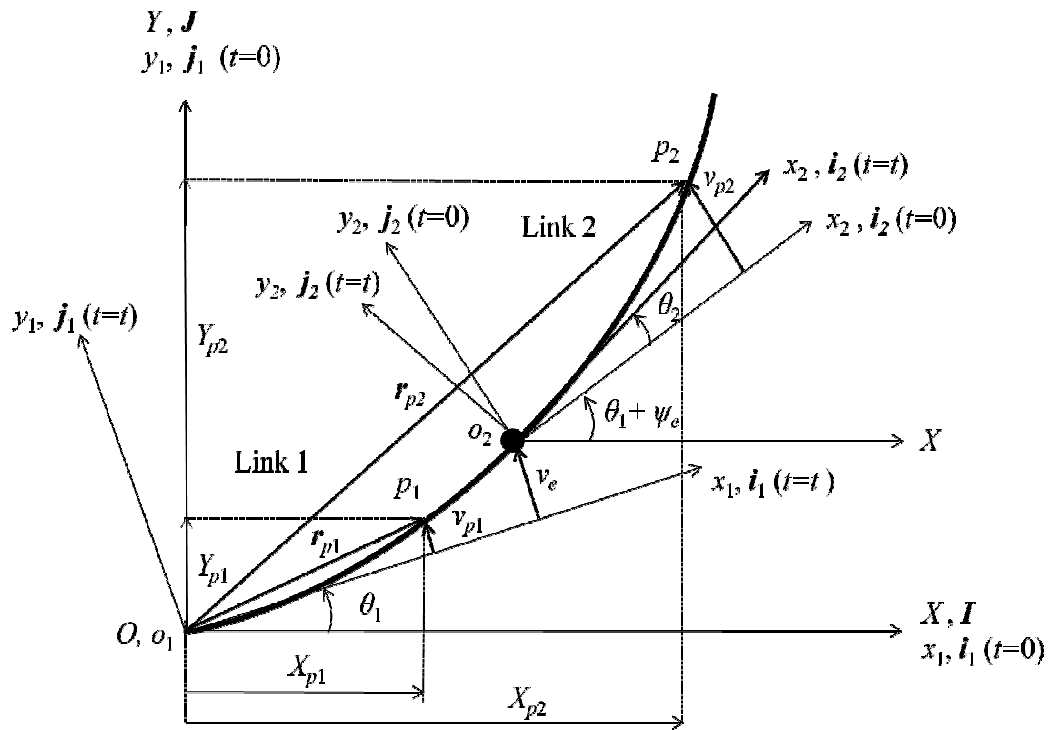
$$X_{p2} = L_1 \cos \theta_1(t) - v_e(x_1, t) \sin \theta_1(t) + x_2 \cos(\theta_1(t) + \psi_e(x_1, t) + \theta_2(t)) - v_{p2}(x_2, t) \sin(\theta_1(t) + \psi_e(x_1, t) + \theta_2(t)) \quad (5)$$

$$Y_{p2} = L_1 \sin \theta_1(t) + v_e(x_1, t) \cos \theta_1(t) + x_2 \sin(\theta_1(t) + \psi_e(x_1, t) + \theta_2(t)) + v_{p2}(x_2, t) \cos(\theta_1(t) + \psi_e(x_1, t) + \theta_2(t)) \quad (6)$$

The velocity vector of the arbitrary points P_1 and P_2 at time $t = t$, shown in Fig.1 is expressed by

$$\dot{\mathbf{r}}_{p1} = \dot{X}_{p1}(x_1, \theta_1, \dot{\theta}_1, v_{p1}, \dot{v}_{p1}, t)\mathbf{I} + \dot{Y}_{p1}(x_1, \theta_1, \dot{\theta}_1, v_{p1}, \dot{v}_{p1}, t)\mathbf{J} \quad (7)$$

$$\dot{\mathbf{r}}_{p2} = \dot{X}_{p2}(x_2, \theta_1, \theta_2, \dot{\theta}_1, \dot{\theta}_2, v_e, \psi_e, v_{p2}, \dot{v}_e, \dot{\psi}_e, \dot{v}_{p2}, t)\mathbf{I} + \dot{Y}_{p2}(x_2, \theta_1, \theta_2, \dot{\theta}_1, \dot{\theta}_2, v_e, \psi_e, v_{p2}, \dot{v}_e, \dot{\psi}_e, \dot{v}_{p2}, t)\mathbf{J} \quad (8)$$



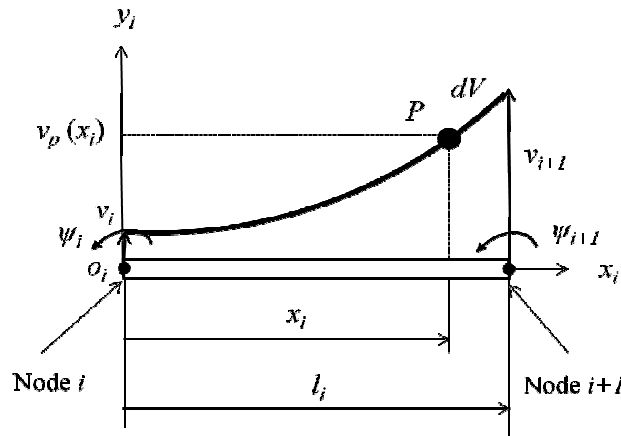
- $O-XY$: Global coordinate frame
- $o_1-x_1y_1$: Rotating coordinate frame fixed to Link 1
- $o_2-x_2y_2$: Rotating coordinate frame fixed to Link 2
- r_{p1}, r_{p2} : Position vectors of the arbitrary points p_1 and p_2 in the X -axis of the $O-XY$
- θ_1 : Rotational angle of the first motor
- θ_2 : Rotational angle of the second motor
- X_{p1}, X_{p2} : Coordinates of the arbitrary points p_1 and p_2 in the X -axis of the $O-XY$
- Y_{p1}, Y_{p2} : Coordinates of the arbitrary points p_1 and p_2 in the Y -axis of the $O-XY$
- v_{p1} : Lateral deformation of the arbitrary point p_1 on Link 1 in the $o_1-x_1y_1$
- v_{p2} : Lateral deformation of the arbitrary point p_2 on Link 2 in the $o_2-x_2y_2$
- ψ_e : Rotational angle of the end-point of Link 1
- v_e : Lateral deformation of the end-point of Link 1
- L_1 : Length of Link 1

Figure 1: Position Vectors of Arbitrary Points P_1 and P_2 in the Global and Rotating Coordinate Frames

Finite Element Method

Figure 2 shows the element coordinate frame of Element i -th, and an arbitrary point P on Element i -th. Here, there are four boundary conditions together at nodes i and $(i+1)$ when the one-dimensional and two-node element is used. The four boundary conditions are expressed as nodal vector as follow

$$\delta_i = \{v_i \quad \psi_i \quad v_{i+1} \quad \psi_{i+1}\}^T \tag{9}$$



$o_i - x_i y_i$: Element coordinate frame of Element i -th

Figure 2: Element Coordinate Frame of Element i -th

Then, the hypothesized deformation has four constants as follows [13]

$$v_i = a_1 + a_2 x_i + a_3 x_i^2 + a_4 x_i^3 \quad (10)$$

where x_i is position coordinate of the arbitrary point P in the x_i -axis of the element coordinate frame. Then, the relation between the lateral deformation v_i and the rotational angle ψ_i of the Node i is given by

$$\psi_i = \frac{\partial v_i}{\partial x_i} \quad (11)$$

Moreover, from mechanics of materials, the strain of Node i can be defined by

$$\varepsilon_i = -y_i \frac{\partial^2 v_i}{\partial x_i^2} \quad (12)$$

where y_i is position coordinate of the arbitrary point P in the y_i -axis of the element coordinate frame.

Equations of Motion

Equations of motion of Element i -th on Link 1 and Link 2 are respectively given by

$$M_i \ddot{\delta}_i + C_i \dot{\delta}_i + [K_i - \dot{\theta}_1^2 M_i] \delta_i = \ddot{\theta}_1 f_i \quad (13)$$

$$M_i \ddot{\delta}_i + C_i \dot{\delta}_i + [K_i - (\dot{\theta}_1 + \dot{\psi}_e + \dot{\theta}_2)^2 M_i] \delta_i = (\ddot{\theta}_1 + \ddot{\psi}_e + \ddot{\theta}_2) f_i + (L_1 \ddot{\theta}_1 + \ddot{v}_e - v_e \dot{\theta}_1^2) \cos(\psi_e + \theta_2) g_i \quad (14)$$

$$+ \left(v_e \ddot{\theta}_1 + L_1 \dot{\theta}_1^2 + \frac{1}{2} \dot{v}_e (3\dot{\theta}_1 - \dot{\psi}_e - \dot{\theta}_2) \right) \sin(\psi_e + \theta_2) g_i$$

where M_i , C_i , and K_i , are the mass matrix, damping matrix, stiffness matrix of Element i -th on Link 1 and Link 2. Vectors of f_i and g_i are the excitation vectors on Link 1 and Link 2. The representation of the matrices and the vector of f_i can be found in [8] and [10]. The vector of g_i can be defined by

$$\mathbf{g}_i = \frac{\rho_i S_i l_i}{12} \{-6 \quad 15l_i \quad 6 \quad l_i\}^T \quad (15)$$

Finally, the equations of motion of Link 1 and Link 2 with n elements considering the boundary conditions is given by

$$\mathbf{M}_n \ddot{\boldsymbol{\delta}}_n + \mathbf{C}_n \dot{\boldsymbol{\delta}}_n + [\mathbf{K}_n - \dot{\theta}_1^2 \mathbf{M}_n] \boldsymbol{\delta}_n = \ddot{\theta}_1 \mathbf{f}_n \quad (16)$$

$$\begin{aligned} \mathbf{M}_n \ddot{\boldsymbol{\delta}}_n + \mathbf{C}_n \dot{\boldsymbol{\delta}}_n + [\mathbf{K}_n - (\dot{\theta}_1 + \dot{\psi}_e + \dot{\theta}_2)^2 \mathbf{M}_n] \boldsymbol{\delta}_n &= (\ddot{\theta}_1 + \ddot{\psi}_e + \ddot{\theta}_2) \mathbf{f}_n + (L_1 \ddot{\theta}_1 + \ddot{v}_e - v_e \dot{\theta}_1^2) \cos(\psi_e + \theta_2) \mathbf{g}_n \\ + (v_e \ddot{\theta}_1 + L_1 \dot{\theta}_1^2 + \frac{1}{2} \dot{v}_e (3\dot{\theta}_1 - \dot{\psi}_e - \dot{\theta}_2)) \sin(\psi_e + \theta_2) \mathbf{g}_n \end{aligned} \quad (17)$$

VALIDATION OF THE FORMULATION

Experimental Model

Figure 3 shows the experimental model of the flexible two-link manipulator. The flexible manipulator consists of two flexible aluminum beams, two clamp-parts, two servo motors and the base. Link 1 and Link 2 are attached to the first and second motors through the clamp-parts. Link 1 and Link 2 are connected through the second motor. Two strain gages are bonded to the position of 0.11 [m] and 0.38 [m] from the origin of the two-link system. The first motor is mounted to the base. In the experiments, the motors were operated by an independent motion controller.

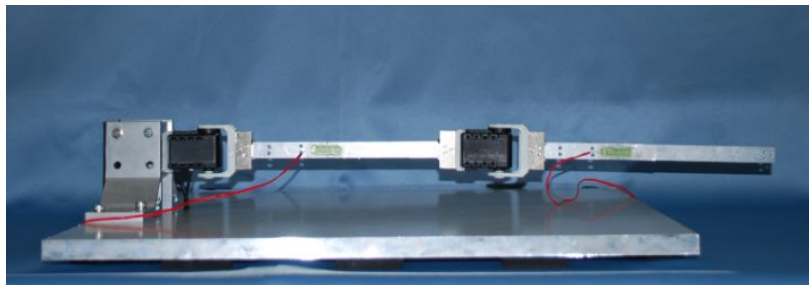


Figure 3: Experimental Model of the Flexible Two-Link Manipulator

Computational Models

In this research, we defined and used five types of computational models of the flexible two-link manipulator.

Model I

A model of only a two-link manipulator was used as Model I. Figure 5.a shows Model I. The links and the clamp-parts were discretized by 35 elements. Two strain gages are bonded to the position of Node 6 and Node 22 of the two-link (0.11 [m] and 0.38 [m] from the origin), respectively.

Model II

A model of the flexible two-link manipulator including one piezoelectric actuator was defined as Model II. Figure 5.b shows model II. The piezoelectric actuator was bonded to the one surface of elements 4. The links including the clamp-parts and the piezoelectric actuator were discretized by 36 elements.

The piezoelectric actuator suppresses the vibration of the two-link flexible manipulator by adding bending moments at nodes 3 and 6 of the two-link manipulator, M_3 and M_6 . The bending moments are generated by applying voltages E_1 to the piezoelectric actuator. The bending moments proportional to the voltage which are expressed by

$$M_3 = -M_6 = d_{11}E_1 \quad (18)$$

Here d_{11} is a constant quantity and M_3 opposites to M_6 .

Furthermore, the voltage to generate the bending moments is proportional to the strains ε_1 of the two-link due to the vibration. The relations can be expressed as follows

$$E_1 = \pm \frac{1}{d_{21}} \varepsilon_1 \quad (19)$$

Here d_{21} is a constant quantity.

Model III

A model of the flexible two-link manipulator including the two piezoelectric actuators was defined as Model III. Figure 5.c shows model III. The piezoelectric actuators were bonded to the one surface of elements 4 and 20. The links including the clamp-parts and the piezoelectric actuators were discretized by 36 elements. Schematic representations on modeling of the piezoelectric actuators are shown in Figure 4. Physical parameters of the flexible two-link manipulator model and the piezoelectric actuators are shown in table 1.

The first piezoelectric actuator suppresses the vibration of the two-link flexible manipulator by adding bending moments at nodes 3 and 6 of the two-link manipulator, M_3 and M_6 . The second piezoelectric actuator suppresses the vibration of the two-link flexible manipulator by adding bending moments at nodes 19 and 22 of the two-link manipulator, M_{19} and M_{22} . The bending moments are generated by applying voltages E_1 and E_2 to the piezoelectric actuators. The bending moments proportional to the voltages which are expressed by Eq. (18) and

$$M_{19} = -M_{22} = d_{12}E_2 \quad (20)$$

Here d_{12} is a constant quantity and M_{19} opposites to M_{22} .

Furthermore, the voltages to generate the bending moments are proportional to the strains ε_1 and ε_2 of the two-link due to the vibration. The relations can be expressed by Eq. (19) and

$$E_2 = \pm \frac{1}{d_{22}} \varepsilon_2 \quad (21)$$

Here d_{22} is a constant quantity. Then, d_{11} , d_{12} , d_{21} and d_{22} will be determined by comparing the calculated results and experimental ones.

Model IV

Figure 5.d shows model IV that an end-effector is considered for a two-link manipulator with a piezoelectric actuator. Model IV is used to show that the proposed control scheme is also suitable for such system. The end-effector is presented by adding a concentrated mass to Model II. In this case, the equation of motion of the tip element containing the

concentrated mass is given by

$$[M_i + M_{icm}] \ddot{\delta}_i + C_i \dot{\delta}_i + [K_i - (\dot{\theta}_1 + \dot{\psi}_e + \dot{\theta}_2)^2 [M_i + M_{icm}]] \delta_i = (\ddot{\theta}_1 + \ddot{\psi}_e + \ddot{\theta}_2) \{f_i + f_{icm}\} + (L_1 \ddot{\theta}_1 + \ddot{v}_e - v_e \dot{\theta}_1^2) \cos(\psi_e + \theta_2) \{g_i + g_{icm}\} + \left(v_e \ddot{\theta}_1 + L_1 \dot{\theta}_1^2 + \frac{1}{2} \dot{v}_e (3\dot{\theta}_1 - \dot{\psi}_e - \dot{\theta}_2) \right) \sin(\psi_e + \theta_2) \{g_i + g_{icm}\} \tag{22}$$

where the vectors of f_{icm} and g_{icm} are given by

$$f_{icm} = m_c \{0 \quad 0 \quad -l_{1-i} - l_i \quad 0\}^T \tag{23}$$

$$g_{icm} = m_c \{0 \quad 0 \quad -1 \quad 0\}^T \tag{24}$$

and the concentrated mass matrix M_{icm} can be expressed as

$$M_{icm} = \begin{bmatrix} 0 & 0 & 0 & 0 \\ 0 & 0 & 0 & 0 \\ 0 & 0 & m_c & 0 \\ 0 & 0 & 0 & 0 \end{bmatrix} \tag{25}$$

where m_c is the mass of the concentrated mass.

Model V

Figure 5.e shows model V that an end-effector is considered for a two-link manipulator with two piezoelectric actuators. Model V is used to show that the proposed control scheme is also suitable for such system. The end-effector is presented by adding a concentrated mass to Model III. In this case, the equation of motion of the tip element containing the concentrated mass is given by Eq. (22)

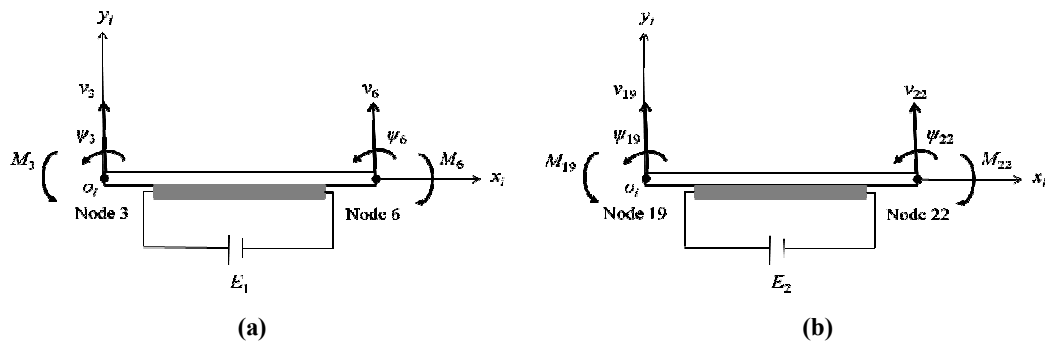
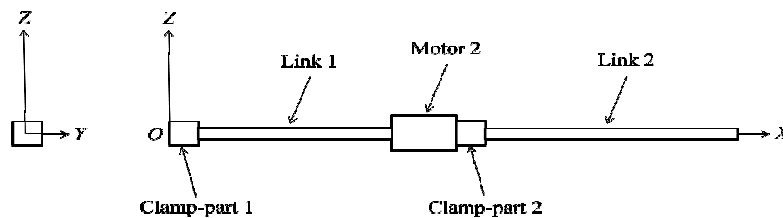
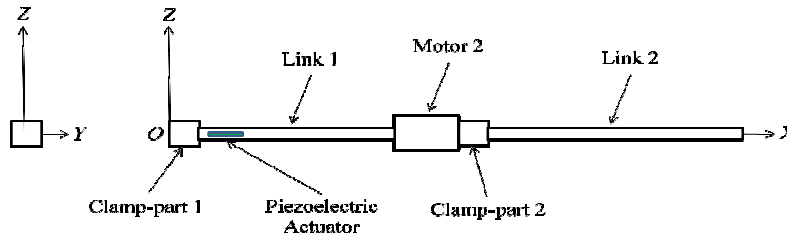


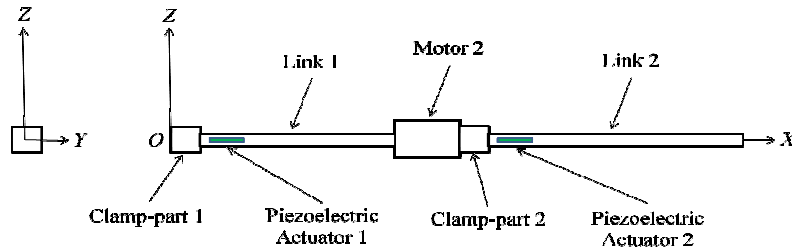
Figure 4: Modeling of Piezoelectric Actuators: (a) Modeling of Actuator 1, (b) Modeling of Actuator 2



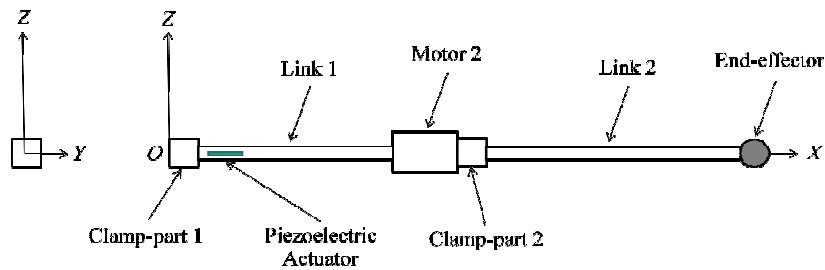
(a) Model I : Only Two-Link



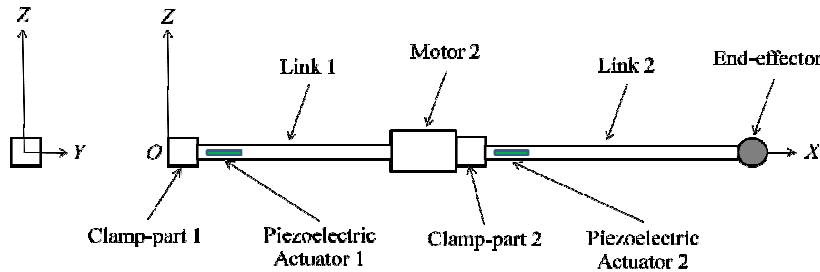
(b) Model II: Two-Link with a Piezoelectric Actuator



(c) Model III: Two-link with Two Piezoelectric Actuators



(d) Model IV: Two-Link with a Piezoelectric Actuator and an End-Effector



(e) Model V: Two-Link with Two Piezoelectric Actuators and an End-Effector

Figure 5: Computational Models of the Flexible Two-Link Manipulator

Table 1: Physical Parameters of the Flexible Two-Link and the Piezoelectric Actuators

l : Total length	m	4.05×10^{-1}
l_1 : Length of Link 1	m	1.90×10^{-1}
l_2 : Length of Link 2	m	2.15×10^{-1}
l_{c1}, l_{c2} : Length of clamp-parts 1 and 2	m	1.50×10^{-2}
l_{a1}, l_{a2} : Length of Actuators 1 and 2	m	2.00×10^{-2}
S_{l1}, S_{l2} : Cross section area of links 1 and 2	m ²	1.95×10^{-5}
S_{c1}, S_{c2} : Cross section area of clamp-parts 1 and 2	m ²	8.09×10^{-4}

S_{a1}, S_{a2} : Cross section area of actuators 1 and 2	m^2	1.58×10^{-5}
I_{z1}, I_{z2} : Cross section area moment of inertia around z -axis of links 1 and 2	m^4	2.75×10^{-12}
I_{zc1}, I_{zc2} : Cross section area moment of inertia around z -axis of clamp-parts 1 and 2	m^4	3.06×10^{-8}
I_{za1}, I_{za2} : Cross section area moment of inertia around z -axis of actuators 1 and 2	m^4	1.61×10^{-11}
E_1, E_2 : Young's Modulus of links 1 and 2	GPa	7.03×10^1
E_{c1}, E_{c2} : Young's Modulus of clamp-parts 1 and 2	GPa	7.03×10^1
E_{a1}, E_{a2} : Young's Modulus of actuators 1 and 2	GPa	4.40×10^1
ρ_1, ρ_2 : Density of links 1 and 2	kg/m^3	2.68×10^3
ρ_{c1}, ρ_{c2} : Density of clamp-parts 1 and 2	kg/m^3	2.68×10^3
ρ_{a1}, ρ_{a2} : Density of actuators 1 and 2	kg/m^3	3.33×10^3
α_1, α_2 : Damping factor of links 1 and 2	s^{-1}	0×10^{-4}
E_1, E_2 : Maximum input voltages of actuators 1 and 2	V	150.00
F_1, F_2 : Maximum output forces of actuators 1 and 2	N	200.00
m_2 : Mass of the second motor	g	113.53

Time History Responses of Free Vibration

Experiment on free vibration was conducted using an impulse force as an external one. Figure 6.a shows the experimental time history response of strains, ϵ_x on the free vibration at the same position in the calculation (0.11 [m] from the origin of the two-link system).

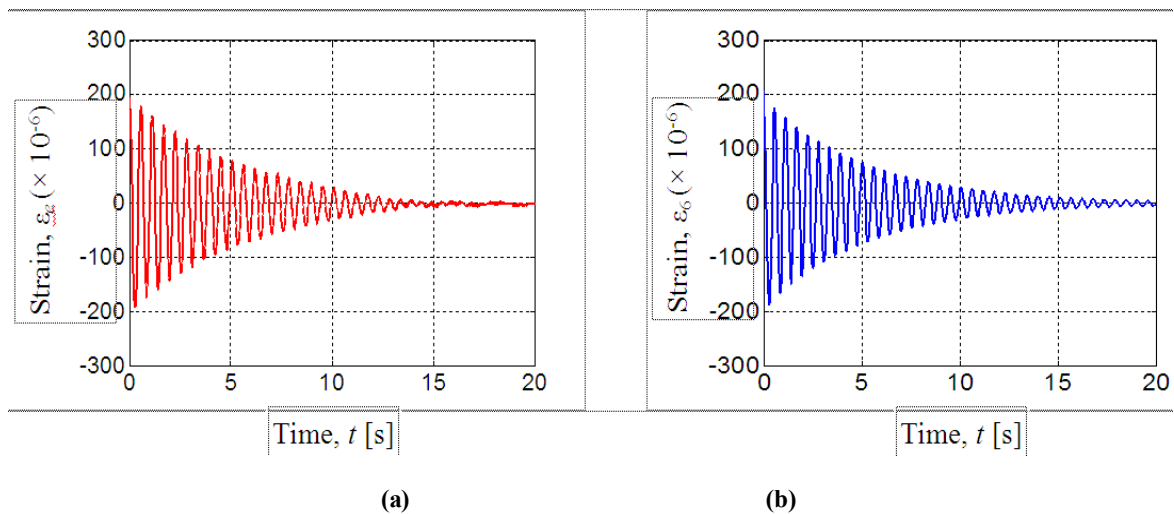


Figure 6: Time History Responses of Strains on Free Vibration: (a) Experimental Strains at 0.11 [m] from the Origin of the Two-Link, (b) Calculated Strains at Node 6 of Model I

Furthermore, the computational codes on time history response of Model I were developed. Figure 6.b shows the calculated strains at Node 6 of Model I under the impulse force.

Time History Responses of Free Vibration

Both the experimental and calculated time history responses of strains on free vibration were transferred by FFT processing to find their frequencies. Figures 7.a and 7.b show the experimental and calculated natural frequencies of the

flexible two-link manipulator, respectively. The first experimental natural frequency, 1.79 Hz agreed with the calculated one, 1.80 Hz. The second experimental natural frequency could not be measured. However, in the calculation, it could be obtained as 8.95 Hz.

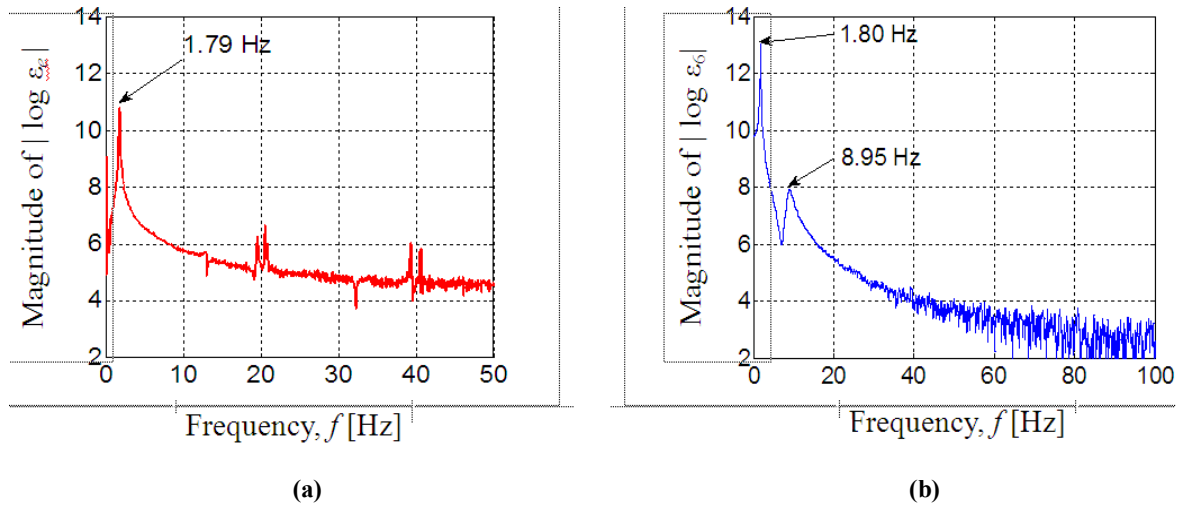
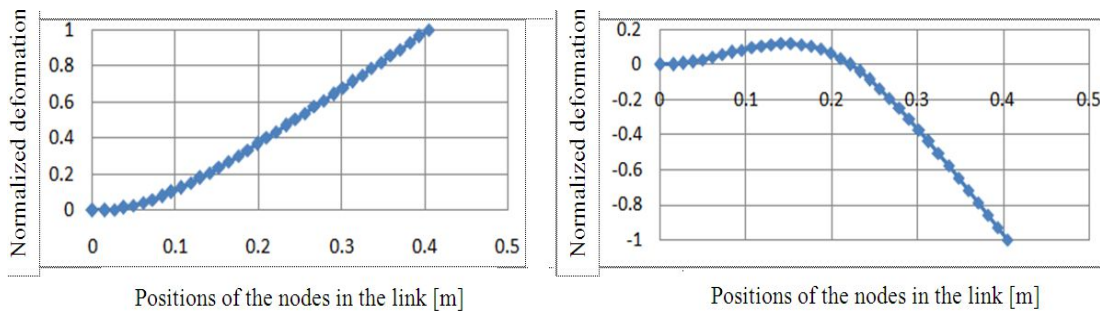


Figure 7: Natural Frequencies: (a) Experimental Natural Frequency of the Flexible Two-Link, (b) Calculated Natural Frequencies of Model I

Eigen-Values and Eigen-Vectors Analysis

The computational codes on Eigen-values and Eigen-vectors analysis were developed for natural frequencies and vibration modes. The calculated results for the first and second natural frequencies were 1.79 Hz and 8.92 Hz, respectively. The vibration modes of natural frequencies are shown in Figure 8.



(b) First Vibration Mode and Natural Frequency ($f_1 = 1.79$ Hz) (a) Second vibration Mode and Natural Frequency ($f_2 = 8.92$ Hz)

Figure 8: Vibration Modes and Natural Frequencies

Time History Responses Due to the Base Excitations

Another experiment was conducted to investigate the vibration of the flexible two-link due to the base excitations generated by rotation of the motors. In the experiment, the motors were rotated by the angle of $\pi/2$ radians (90 degrees) within 0.50 [s]. Figures 11.a and 12.a show the experimental time history responses of strains of the flexible two-link due to the motors’ rotation at 0.11 [m] and 0.38 [m] from the origin of the link, respectively. Furthermore, based on Figures 11.a and 12.a, the time history response of strains at Node 6 and Node 22 of Model I were calculated as shown in Figures 11.b and 12.b, respectively.

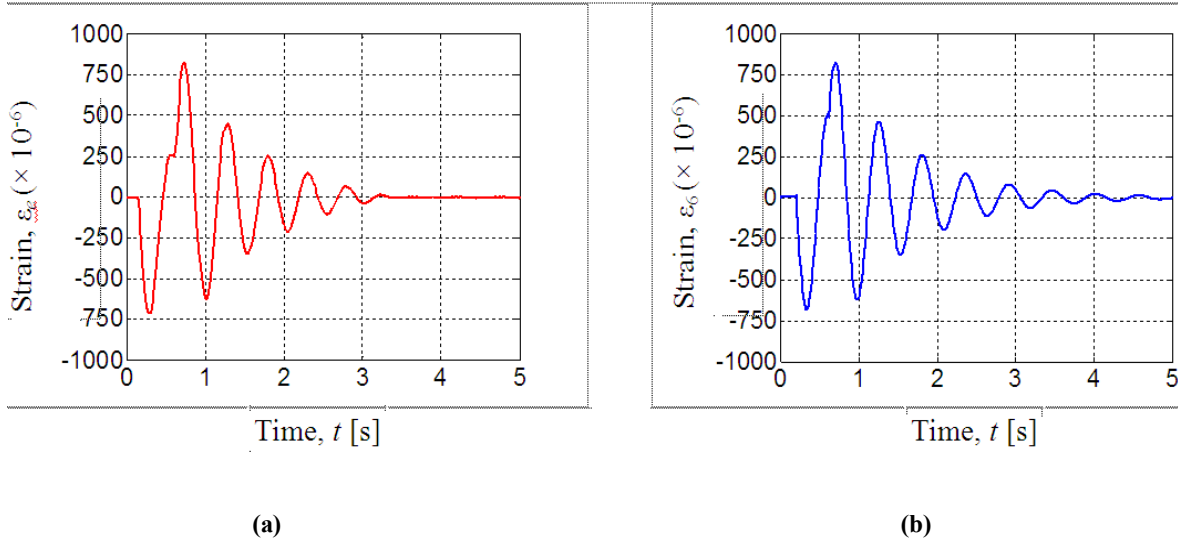


Figure 11: Time History Responses of Strains Due to Base Excitation: (a) Experimental Strains at 0.11 [m] from the Origin of the Two-Link, (b) Calculated Strains at Node 6 of Model I

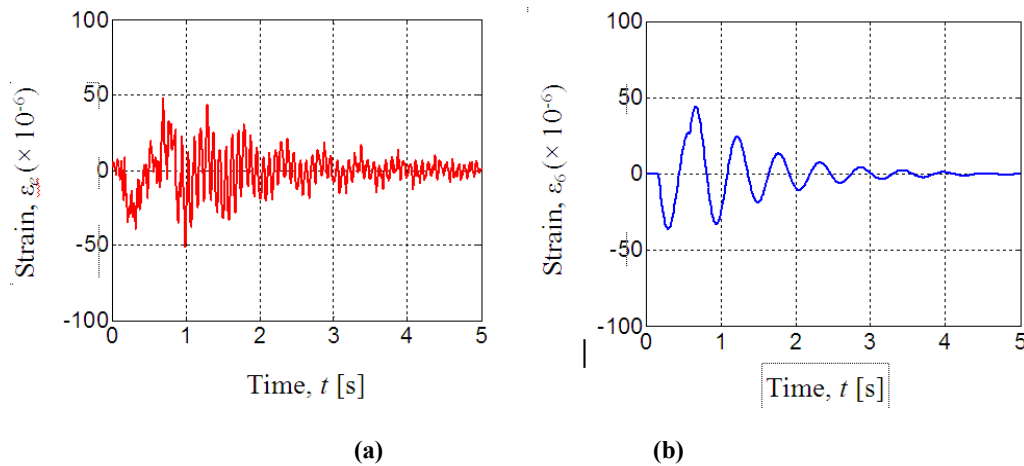


Figure 12: Time History Responses of Strains Due to Base Excitation: (a) Experimental Strains at 0.38 [m] from the Origin of the Two-Link, (b) Calculated Strains at Node 22 of Model I

CONTROL SCHEME AND SIMULATIONS

Control Scheme

A control scheme to suppress the vibration of the two-link system was designed using one and two piezoelectric actuators. It was done by adding bending moments generated by the piezoelectric actuators to the two-link system. To drive the actuators, two proportional-derivative (PD) controllers have been designed and examined.

Using a Piezoelectric Actuator

The piezoelectric actuator suppresses the vibration of the two-link flexible manipulator by adding bending moments at nodes 3 and 6 of the two-link manipulator, M_3 and M_6 . Therefore, the equation of motion of Link 1 become

$$M_n \ddot{\delta}_n + C_n \dot{\delta}_n + [K_n - \dot{\theta}_1^2 M_n] \delta_n = \dot{\theta}_1 f_n + u_{1n} \tag{26}$$

where the vector of \mathbf{u}_{1n} containing M_3 and M_6 is the control force generated by the actuator to the two-link system.

Furthermore, substituting Eq. (19) to Eq. (18) gives

$$M_3, M_6 = \pm \frac{d_{11}}{d_{21}} \varepsilon_1 \quad (27)$$

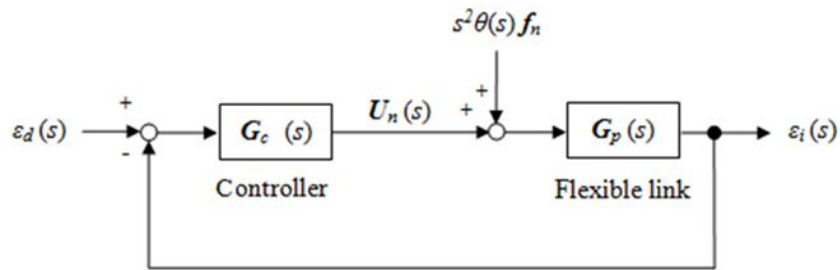
Based on Eq. (27) the control force can be defined in s -domain as follows

$$U_{1n}(s) = G_{C1}(s)(\varepsilon_d(s) - \varepsilon_6(s)) \quad (28)$$

where ε_d and ε_6 denote the desired and measured strains at Node 6, respectively. The gain of PD-controller can be written by a vector in s -domain as follows

$$G_{C1}(s) = \{0 \quad 0 \quad 0 \quad K_{p1} + K_{d1}s \quad 0 \quad -(K_{p1} + K_{d1}s) \quad 0 \quad \dots \quad 0\}^T \quad (29)$$

A block diagram of the PD-controls for the two-link system using one actuator is shown in Figure 13.



ε_d : Desired strain
 F : Base excitations
 ε_i : Measured strains at Node 6
 U_n : Bending moments
Figure 13: Block Diagram of PD-Controller of the Flexible Two-Link Manipulator Using a Piezoelectric Actuator

Using Two Piezoelectric Actuators

The first piezoelectric actuator suppresses the vibration of the two-link flexible manipulator by adding bending moments at nodes 3 and 6 of the two-link manipulator, M_3 and M_6 , as explained in sub-chapter 4.1.1. The second piezoelectric actuator suppresses the vibration of the two-link flexible manipulator by adding bending moments at nodes 19 and 22 of the two-link manipulator, M_{19} and M_{22} . Therefore, the equation of motion of Link 1 is shown in Eq. (26) and the equation of motion of Link 2 is given by

$$\mathbf{M}_n \ddot{\boldsymbol{\delta}}_n + \mathbf{C}_n \dot{\boldsymbol{\delta}}_n + \left[\mathbf{K}_n - (\dot{\theta}_1 + \dot{\psi}_e + \dot{\theta}_2)^2 \mathbf{M}_n \right] \boldsymbol{\delta}_n = (\ddot{\theta}_1 + \ddot{\psi}_e + \ddot{\theta}_2) \mathbf{f}_n + (L_1 \ddot{\theta}_1 + \ddot{v}_e - v_e \dot{\theta}_1^2) \cos(\psi_e + \theta_2) \mathbf{g}_n \quad (30)$$

$$+ \left(v_e \ddot{\theta}_1 + L_1 \dot{\theta}_1^2 + \frac{1}{2} \dot{v}_e (3\dot{\theta}_1 - \dot{\psi}_e - \dot{\theta}_2) \right) \sin(\psi_e + \theta_2) \mathbf{g}_n + \mathbf{u}_{2n}$$

where the vector of \mathbf{u}_{2n} containing M_{19} and M_{22} is the second control force generated by the second piezoelectric actuator to the two-link system.

Furthermore, substituting Eq. (21) to Eq. (20) gives

$$M_{19}, M_{22} = \pm \frac{d_{12}}{d_{22}} \varepsilon_2 \quad (31)$$

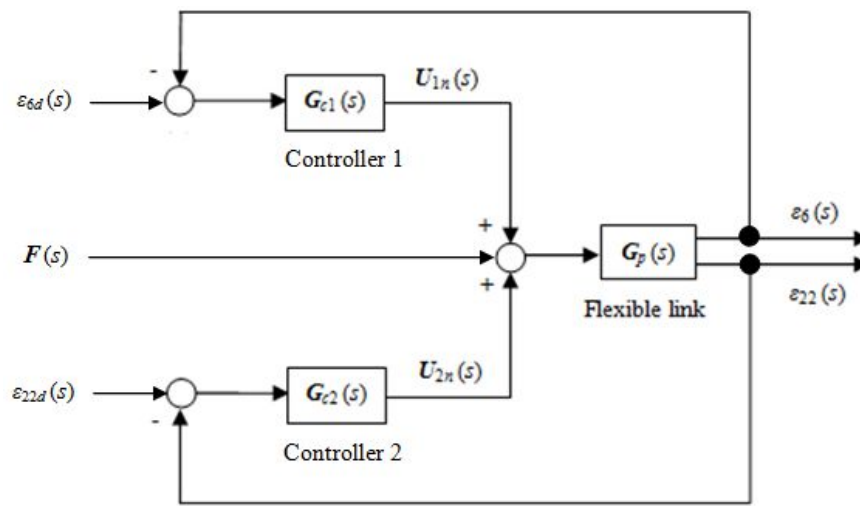
Based on Eq. (31) the second control force can be defined in s -domain as follows

$$U_{2n}(s) = \mathbf{G}_{C2}(s)(\varepsilon_d(s) - \varepsilon_{22}(s)) \quad (32)$$

where ε_d and ε_{22} denote the desired and measured strains at Node 22, respectively. The gain of the second PD-controller can be written by a vector in s -domain as follows

$$\mathbf{G}_{C2}(s) = \{0 \ 0 \ 0 \ K_{p2} + K_{d2}s \ 0 \ -(K_{p2} + K_{d2}s) \ 0 \ \dots \ 0\}^T \quad (33)$$

A block diagram of the PD-controls for the two-link system using one actuator is shown in Fig. 14.



ε_d : Desired strain ε_6 and ε_{22} : Measured strains at nodes 6 and 22
 F : Base excitations U_{1n} and U_{2n} : Bending moments generated by actuator 1 and 2

Figure 14: Block Diagram of PD-Controllers of the Flexible Two-Link Manipulator Using Two Piezoelectric Actuators

Calculated Results

Time history responses of strains at Node 6 and Node 22 on the uncontrolled and controlled system were calculated for Models II, III, IV and V when the first and second motors rotated $\pi/4$ radians (45 degrees) and $\pi/2$ radians (90 degrees) within 0.50 [s], respectively. Time history responses of strains on the controlled system for Models III and IV were calculated under control scheme shown in Figure 13. Time history responses of strains on the controlled system for Models III and V were calculated under control scheme shown in Figure 14. The concentrated mass, m_c used as the end-effector is 14.49 [g].

Examining several gains of the PD-controller using one actuator led to $K_p = 2$ [Nm] and $K_d = 0.6$ [Nms] as the better ones. Furthermore, examining several gains of the PD controllers of the controlled system using two actuators led to $K_{p1} = 2$ [Nm], $K_{d1} = 0.6$ [Nms], $K_{p2} = 40$ [Nm] and $K_{d2} = 10$ [Nms] as the better ones. The controller gains were

examined considering the maximum output forces of the actuators. Figures 15, 16, 17 and 18 show the uncontrolled and controlled time history responses of strains for Models II, III, IV and V, respectively.

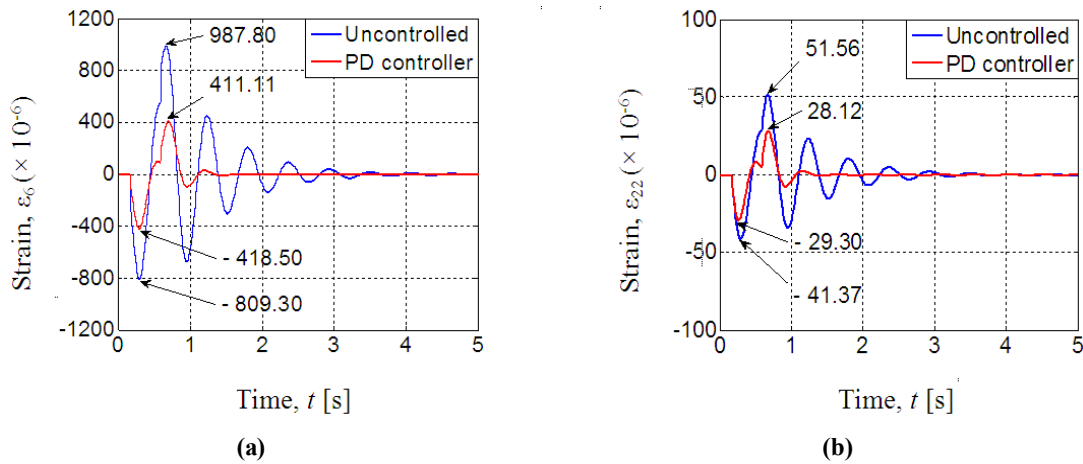


Figure 15: Calculated Time History Responses of Strains for Model II Due to the Base Excitations: (a) at Node 6, (b) at Node 22

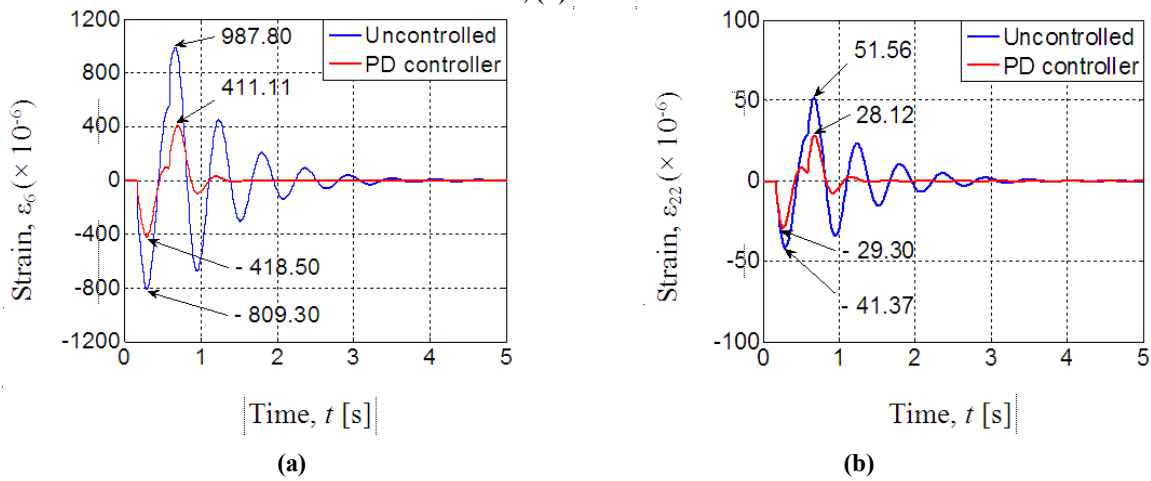


Figure 16: Calculated Time History Responses of Strains for Model III Due to the Base Excitations: (a) at Node 6, (b) at Node 22

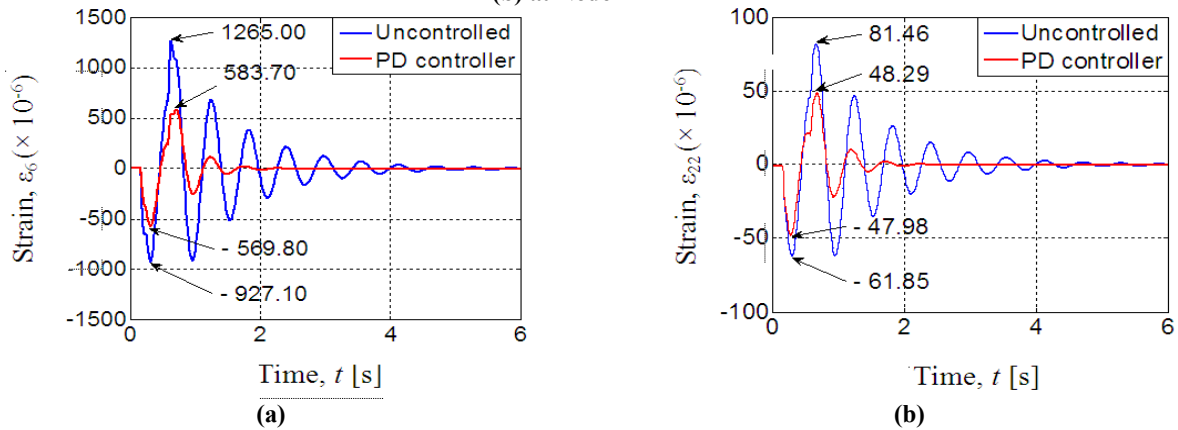


Figure 17: Calculated Time History Responses of Strains for Model IV Due to the Base Excitations: (a) at Node 6, (b) at Node 22

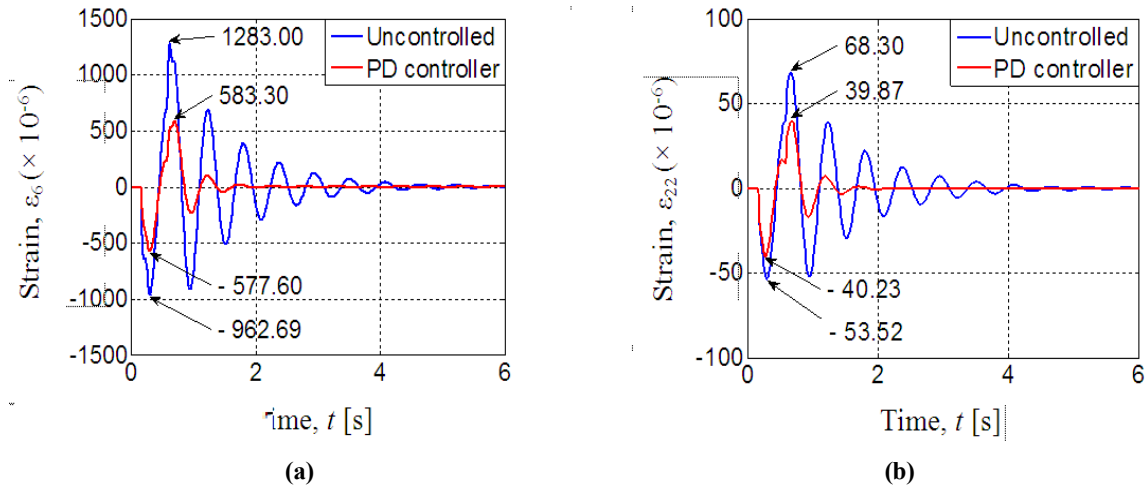


Figure 18: Calculated Time History Responses of Strains for Model V Due to the Base Excitations: (a) at Node 6, (b) at Node 22

The maximum strains of uncontrolled system for Model II at Node 6 and Node 22 were 948.30×10^{-6} and 58.55×10^{-6} , respectively. By using PD-controller they become 453.50×10^{-6} and 39.13×10^{-6} , respectively, as shown in figures 15.a and 15.b. The maximum strains of uncontrolled system for Model III at Node 6 and Node 22 were 987.80×10^{-6} and 51.56×10^{-6} , respectively. By using PD-controller they become 418.50×10^{-6} and 29.30×10^{-6} , respectively, as shown in figures 16.a and 16.b.

Moreover, the maximum strains of uncontrolled system for Model IV at Node 6 and Node 22 were 1265.00×10^{-6} and 81.46×10^{-6} , respectively. By using PD-controller they become 583.70×10^{-6} and 48.29×10^{-6} , respectively, as shown in figures 17.a and 17.b. The maximum strains of uncontrolled system for Model V at Node 6 and Node 22 were 1283.00×10^{-6} and 68.30×10^{-6} , respectively. By using PD-controller they become 583.30×10^{-6} and 39.87×10^{-6} , respectively, as shown in figures 18.a and 18.b.

It was verified from these results that the proposed control scheme can effectively suppress the vibration of the flexible two-link manipulator.

CONCLUSIONS

The equations of motion for the flexible two-link manipulator had been derived using the finite element method. Computational codes had been developed in order to perform dynamics simulations of the system. Experimental and calculated results on time history responses, natural frequencies and vibration modes show the validities of the formulation, computational codes and modeling of the system. Two proportional-derivative controllers were designed to suppress the vibration of the system. The calculated results have been revealed that the vibration of the system can be suppressed effectively even though using only one piezoelectric actuator.

REFERENCES

1. C. Nishidome, and I. Kajiwara, "Motion and Vibration Control of Flexible-link Mechanism with Smart Structure", *JSME International Journal*, Vol.46, No.2, 2003, pp. 565 – 571.

2. Y. Yaman et al, "Active Vibration Control of a Smart Beam", *Proceedings of the 2001 CANSMART Symposium*, 2001, pp. 125 – 134.
3. O.F. Kircali et al, "Active Vibration Control of a Smart Beam by Using a Spatial Approach", *New Developments in Robotics, Automation and Control*, 2009, pp. 378 – 410.
4. J. Zhang et al, "Active Vibration Control of Piezoelectric Intelligent Structures", *Journal of Computers*, Vol. 5. No. 3, 2010, pp. 401 – 409.
5. K. Gurses et al, Vibration control of a single-link flexible manipulator using an array of fiber optic curvature sensors and PZT actuators, *Mechatronics* 19, 2009, pp. 167 – 177.
6. S.X. Xu and T.S. Koko, "Finite Element Analysis and Design of Actively Controlled Piezoelectric Smart Structures", *Finite Elements in Analysis and Design* 40, 2004, pp. 241 – 262.
7. Z.K. Kusculuoglu et al, "Finite Element Model of a Beam with a Piezoceramic Patch Actuator", *Journal of Sound and Vibration* 276, 2004, pp. 27 – 44.
8. A.K. Muhammad., S. Okamoto., & J.H. Lee. (2014). Computer simulations on vibration control of a flexible single-link manipulator using finite-element method. *Proceeding of 19th International Symposium of Artificial Life and Robotics*, 381 – 386.
9. A.K. Muhammad., S. Okamoto., & J.H. Lee. (2014). Computer simulations and experiments on vibration control of a flexible link manipulator using a piezoelectric actuator. *Lecture Notes in Engineering and Computer Science: Proceeding of The International MultiConference of Engineers and Computer Scientists* 2014, 262 – 267.
10. A.K. Muhammad., S. Okamoto., & J.H. Lee. (2014). Comparison of proportional-derivative and active-force controls on vibration of a flexible single-link manipulator using finite-element method. *Journal of Artificial Life and Robotics*, 19:4, 375 – 381. doi: 10.1007/s10015-014-0186-5 A.K. Muhammad., S. Okamoto., & J.H. Lee. (2014). Comparisons of proportional and active-force controls on vibration of a flexible link manipulator using a piezoelectric actuator through calculations and experiments. *Engineering Letters*, 22:3, 134 – 141.
11. A.K. Muhammad., S. Okamoto., & J.H. Lee. (2015). Active-force control on vibration of a flexible single-link manipulator using a piezoelectric actuator. In G.-C. Yang., S.-I. Ao., X. Huang., & O. Castillo (Eds.), *Transactions on Engineering Technologies, 2014*, (pp. 1 – 15). Springer. doi: 10.1007/978-94-017-9588-3_1
12. M. Lalanne., P. Berthier., & J.D. Hagopian. (1983), *Mechanical Vibration for Engineers*, (pp. 146 – 153). John Wiley & Sons Ltd.

